\$ SUPER

Contents lists available at ScienceDirect

Applied Thermal Engineering

journal homepage: www.elsevier.com/locate/apthermeng





Impact of fin geometry and surface roughness on performance of an impingement two-phase cooling heat sink

Cong Hiep Hoang ^{a,*}, Najmeh Fallahtafti ^a, Srikanth Rangarajan ^{a,*}, Ahmad Gharaibeh ^a, Yaser Hadad ^a, Charles Arvin ^b, Kamal Sikka ^b, Scott N. Schiffres ^a, Bahgat Sammakia ^a

ARTICLE INFO

Keyword:
Microchannel
Flow boiling
Pin fins
Jet impingement
Dielectric coolant
Heat sink
Thermal resistance

ABSTRACT

Jet impingement two-phase cooling is often used to handle the high heat fluxes of high-performance electronics. While much of the literature focuses on thermal–hydraulic performance, the effects of fin geometry on the two-phase heat transfer and pressure drop have not been thoroughly investigated. This study was undertaken to examine those factors more closely. The thermal–hydraulic performance of a two-phase cooling impingement heat sink was studied for three different fin configurations: microchannel, pin fin array, and bare copper surface. A copper block with a top surface area of $1^{\prime\prime}\times1^{\prime\prime}$ was used to mimic computer chip. A dielectric coolant Novec/HFE 7000 was used to study flow boiling heat transfer. It was observed that when the original microchannel heat sink was cut into pin fin array heat sink, thermal performance was improved by 51% and pressure drop decreased by 18%. The pin fin array heat sink performs better than the microchannel heat sink and the bare copper surface heat sink. Effects of enhanced surface roughness was also studied with 9% of improvement in thermal performance of a bare copper surface. Comparison with existing literature correlations for pool boiling and flow boiling led to mean absolute error below 12.8%, so a new correlation was developed that has a mean absolute error of 2.4%.

1. Introduction

Electronics cooling is a growing concern for both industry and government organizations. Global data centers consumed around 200 billion kWh/year [1], which corresponded to 1.3% of total global electricity usage. Of this, cooling was reported to consume roughly 33% of the total energy used in legacy data centers [2]. The energy consumption of data centers in the United States increased by 4% from 2014 to 2020, reaching 73 billion kWh in 2020 [3]. Increasing power densities, which are thought to be due to the rise of Artificial Intelligence (AI), high-performance computing (HPC), and machine learning, can lead to increases in the cost and complexity of thermal management. Going forward, more effective solutions for cooling electronic devices will be necessary to overcome increasing energy consumption. State of the art electronics produce heat fluxes that already exceed the capability of air-cooled heat sinks. Given the high specific heat and latent heat of liquid coolants relative to air cooling, liquid cooling is an attractive solution. An IBM study [4] showed that the efficiency of liquid cooling

can be up to 3500 times higher than that of air cooling. Single-phase cooling with water is the most popular liquid cooling method in data center because it has high figure of merit [5–13]. It is reported that the highest heat transfer rate of single-phase cooling heat sink with water can be up to 1150 W for a 27 cm² chip [14,15]. Although having high thermal performance, single-phase cooling also has disadvantages such as high temperature gradient along the chip surface and potential consequences in the event of a fluid leak. By combining a non-conductive dielectric refrigerant with boiling heat transfer, pumped two-phase cooling can enable increased power densities for high power electronics by more than 2x over traditional water/glycol systems [14,16], while eliminating the shorting risks from a fluid leak. Two-phase cooling not only surpasses the basic cooling configurations in heat dissipation rate, but it also provides better surface temperature uniformity due to the boiling of coolant at only slightly above the saturation temperature.

Geometry of the two-phase cold plate has drawn attention from scientists and engineers because it affects both thermal and hydraulic performance [17–25,35]. Law and Lee [17] experimentally studied flow boiling heat transfer in straight- and oblique-finned microchannels. It

E-mail addresses: hhoang2@binghamton.edu (C.H. Hoang), srangar@binghamton.edu (S. Rangarajan).

^a Department of Mechanical Engineering, State University of New York at Binghamton, Binghamton, NY, USA

b IBM Corporation, NY, USA

^{*} Corresponding authors.

Nomeno	clature	$t_{\rm b}$	base thickness of the heat sink
		W_{ch}	channel width of microchannel
Nu	Nusselt number	R_{th}	specific thermal resistance, Kcm²/W
Re	Reynolds number	V_j	volumetric flow rate, m ³ /s
Pr	Prandtl number	ΔP	pressure drop, kPa
Q	input power (W)	EDM	electrical discharge machining
q"	heat flux, W/cm ²	L/min	liter per minute
A _{hs}	heat source area, cm ²	MC	microchannel
A	area covered by microchannels	PFA	pin fin array
To	ambient temperature, °C	$\mu_{ m L}$	viscosity of liquid (N.s/m²)
$T_{\rm w}$	wall temperature, °C	u	liquid velocity (m/s)
Tin	coolant inlet temperature, °C	h_{fg}	latent heat (J/kg)
T _{out}	coolant outlet temperature, °C	$ ho_{ m L}$	liquid density (Kg/m³)
T _{sat}	saturation temperature, °C	$\rho_{\mathbf{v}}$	vapor density (Kg/m³)
P _{in}	pressure at inlet of heat sink, Kpa	M	molar mass of the coolant (kg/kmol)
P _{out}	pressure at outlet of heat sink, Kpa	ΔT	subcooling (°C)
P _{crit}	critical pressure, Kpa	Во	boiling number
P_{r}	reduced pressure, Kpa	$\mathrm{D_{h}}$	hydraulic diameter (m)
h	heat transfer coefficient (Kw/m ² K)	${\sf h}_{1 \varphi}$	single-phase heat transfer contribution
CHF	critical heat flux (W/cm²)	$h_{2\varphi}$	two-phase heat transfer contribution
L/min	liter per minute	IT	information technology
C_{pl}	specific heat of liquid, J/Kg.K	D_{mc}	diameter of area covered by microchannels
d_n	nozzles (jets) diameter, m	$C_{\rm sf}$	coefficient of surface-fluid combination
Wg	gap between two adjacent pin fin arrays (mm)	Greek sy	mhole
L_{p}	pin length (mm)	α	nondimensional forms of heat flux
k_l	thermal conductivity of liquid, W/m-K	heta heta heta	nondimensional form of inlet temperature
L	distance between nozzle (jet) and base, m	O	nondimensional form of finet temperature
t_f	fin thickness of microchannel (mm)	Subscrip	ts
h_{f}	fin height (mm)	in	channel inlet
M	molar mass of the fluid, Kg/Kmol	1	liquid
Rp	roughness in microns	out	channel outlet
L_h	crossflow distance of each nozzle (m)	sat	saturated temperature
σ	surface tension (N/m)	b	base
$Nu_{1\varphi}$	Nusselt number of single-phase contributions		
Nu _{2φ}	Nusselt number of evaporation contributions		

was reported that increments of 2.5-2.8 times in the critical heat flux (CHF) are observed for the oblique fins in the experiments, which contributed to the more stable flow boiling process offered by the oblique fins. Heat transfer performance of the oblique-finned microchannels were 1.2 to 6.2 times higher than straight finned microchannels. However, pumping power of oblique fins is 1.7 times higher than straight fins. Zhang et al. [18] studied reentrant cavity networks produced by wire electric discharge machining at different inlet subcooling. It was found this system yielded high heat transfer coefficient and low pressure drop at low and medium subcooling. Moreover, the interconnected microchannel net can also significantly mitigate the twophase flow instability due to the unique reentrant and segmented structure characteristics. Wan et al. [19] experimentally investigated performance of four types of pin fins in two-phase cooling: square, circular, diamond and streamline. Test results showed that the square micro pin fins presented the best boiling heat transfer, followed by circular and streamline ones. Sempértegui-Tapia and Ribatski [20] investigated saturated flow boiling of R134a for circular, square and triangular tubes with the same external perimeter. It was observed that circular channels showed the best heat transfer performance at low heat fluxes, while for higher heat fluxes triangular channel was the best one. The effect of channel dimensions and mass flux on flow boiling heat transfer of FC-77 through microchannel heat sink has been experimentally investigated in a study by [21]. For a fixed wall heat flux, the heat transfer coefficient is independent of channel width for microchannels of width 400 µm and larger and has a weak dependence on channel width for smaller microchannels down to at least 100 µm. However, for a given

amount of heat dissipation from the heat source, the heat transfer coefficient increases with increasing channel width. The maximum heat that can be removed from the chip increases with decreasing channel width. Also, for a given amount of heat dissipation from the chip, the wall temperature is lower for the smaller channels.

Surface characteristics play an important role in two phase heat transfer. Surface modification can result in higher nucleate density and higher surface contact between fluid and solid surface; therefore, thermal performance of singe-phase and two-phase heat sink can be improved via surface modification. Many recent researches focused on how surface modification techniques to improve thermal performance [26-32]. Zhu et al. [26] designed and fabricated microchannels with well-defined silicon micropillar arrays on the bottom of a heated microchannel wall. The micro pillars have diameter from 5 to 10 µm, height of 25 μm, and pitch from 10 to 40 μm. The aim was to promote capillary flow for thin film evaporation while facilitating nucleation from the sidewalls only. The test results showed that the arrays enhanced critical heat flux by 57 % compared to the smooth surface. Both temperature and pressure drop fluctuation was reduced especially at high heat fluxes. Sitar et al. [27] studied nucleate pool boiling heat transfer on etched and laser structured silicon surfaces. The highest enhancement (244%) of nucleate boiling heat transfer on the silicon sample was achieved by deep reactive ion etching of nucleation cavities with a 30 mm diameter and a 0.125 mm pitch. It was shown that the boiling phenomena initiated at lower superheat when the sample was laser treated or etched.

Jet impingement boiling of the dielectric coolant HFE-7000 has been presented in several works recently. Novec/HFE 7000 is a coolant with a

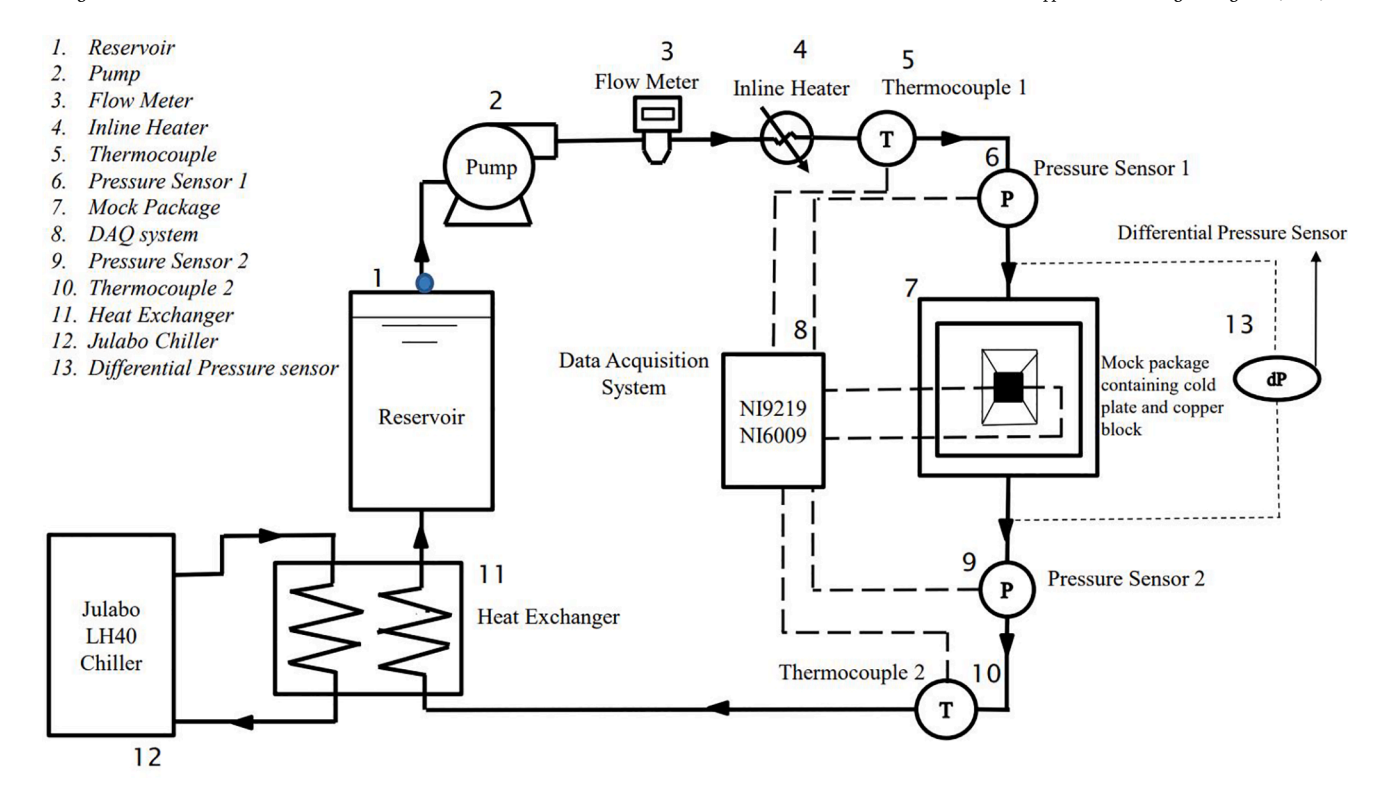


Fig. 1. Schematic diagram of the setup.

low global warming potential and a low boiling point of 34 °C at 1 atm. Its low boiling point and low pressure allows IT equipment operation at low junction temperature and acceptable pumping power. Cui et al. [33] studied two-phase flow instability in distributed jet array impingement on a pin-finned surface. The results show that two-phase instabilities can be delayed by increasing flow rates, but the degree of instability cannot be reduced once it occurs. These instabilities can also be attenuated or even eliminated by decreasing jet-to-target distance or enlarging spray ports. Heat transfer characteristics of normal and distributed jet arrays on smooth surfaces and pin-fin surfaces with coolant HFE 7000 was presented in [34]. It was observed that the boiling instability had no detrimental effects because it only led to a slight drop in heat transfer coefficient and would not lead to earlier occurrence of CHF. The authors previously studied effects of flow rate, subcooling, heat flux and fin height on thermal performance and pumping power of a two-phase cooling microchannel heat sink [35]. The results show that thermal performance can be improved 46 % by varying microchannel fin height and without changing pumping power significantly. Nucleate boiling is the dominant mechanism; therefore, thermal performance is highly dependent on heat flux and weakly dependent on flow rate. Number of works on jet impingement boiling with Novec/HFE 7000 is limited [33–38] and more studies are demanded for enhancement of knowledge in this area.

Generally, the previous studies of jet impingement boiling with various coolants focused on either microchannel or pin fins. Considering that most studies were systematic in nature, they did not provide a more universal understanding of the effect of fin geometries on the heat transfer coefficient and pressure drop. Therefore, the objective of the present work is to compare the performance of different fin geometries

and study the effects of surface roughness on the boiling heat transfer of an impingement heat sink with a dielectric coolant Novec/HFE 7000. Three geometries were investigated in this study including microchannel, pin fin arrays and bare copper surface. In addition, the heat transfer coefficients obtained in this work are compared to values predicted using existing correlations for pool boiling and flow boiling.

2. Experimental setup and procedures

2.1. Flow loop and test section

Flow boiling experiments are conducted in a closed loop, as depicted in Fig. 1. The setup is previously described in detail [35,39]. Novec/HFE 7000 was chosen as the working fluid. The thermophysical properties of Novec/HFE 7000 is presented in Table 2.

In the mock package (Fig. 2), a copper block was used to mimic computer chip with top surface area of $1^{\circ}x1^{\circ}$. The copper block was placed on top of a ceramic fiber sheet and heat sink was placed on top of the copper block top surface. A thermal paste (Kryonaut Thermal-Grizzly) with thermal conductivity of 12.5 W/m-K was used as thermal interface material between heat sink and copper block top surface. Weights were placed on the weight seat for maintaining pressure around 15 psi and uniform interfacial thickness. The heat input of the copper block was provided using four cartridge heaters (Omega CIR3020/120 V) installed in the bottom portion of the copper block. Each cartridge heater can deliver 400 W of heating. The whole mock package was insulated with layers of fiber glass and then placed inside a polystyrene box for minimizing convection.

Table 2The thermophysical properties of the working fluid Novec/HFE 7000.

Reference temperature (°C)	Coolant	Specific Heat (kJ/kg°C)	Viscosity (Pa. s)	Thermal conductivity (W/m-K)	Boiling point at 1 atm (°C)	Heat of vaporization (kJ/kg)
20 °C	Novec/HFE 7000	1.3	4.5×10^{-4}	0.075	34	142

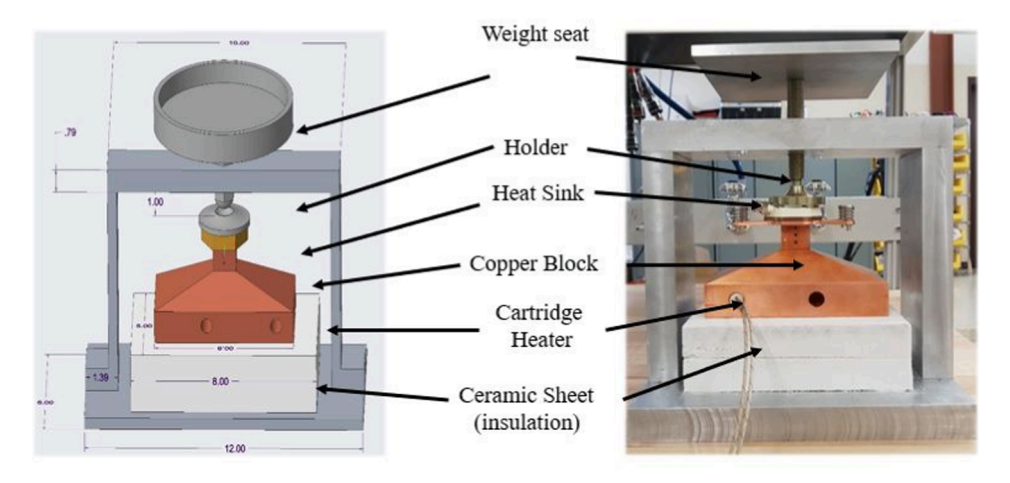


Fig. 2. Mock Package.

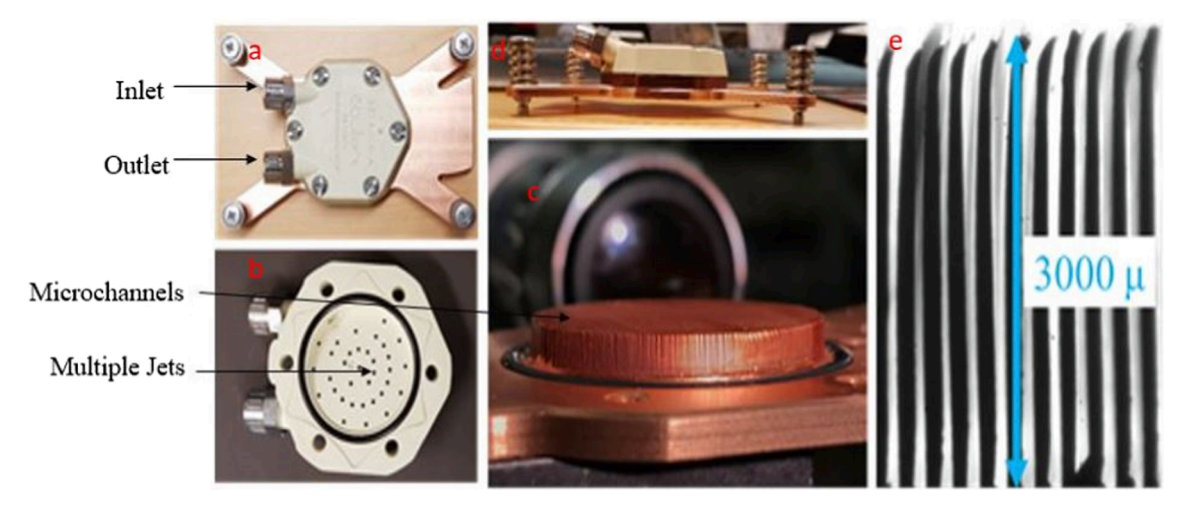


Fig. 3. Heat sink design a) top view b) multiple jets c) microchannels d) side view of the entire cold plate e) microscope picture of the microchannels (side view).

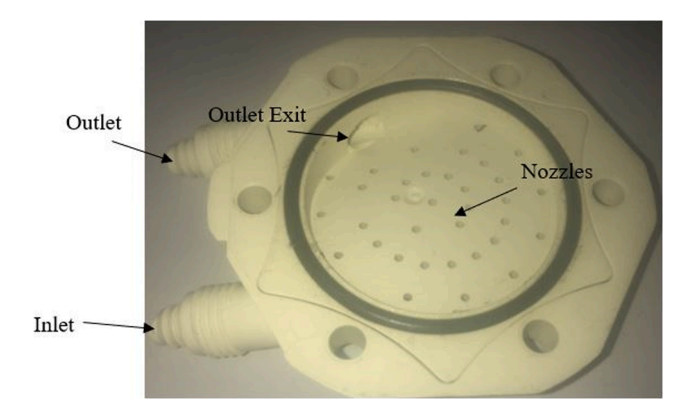


Fig. 4. Lid with inlet, nozzles (jets) and outlet. Each jet has diameter of 1 mm and there are 34 jets.

2.2. Heat sink design and manufacturing

Heat sink design acquired from a commercial company [36] was presented in Fig. 3. The cap design was presented in Fig. 4. The original heat sink consists of microchannels, multiple jets, inlet and outlet. There are 34 jets with diameter of 1 mm for each jet. Microchannel width and fin thickness are both 0.1 mm and fin height were 3 mm. The distance between the fin tip and the jet plate is 0.3 mm as mentioned in our

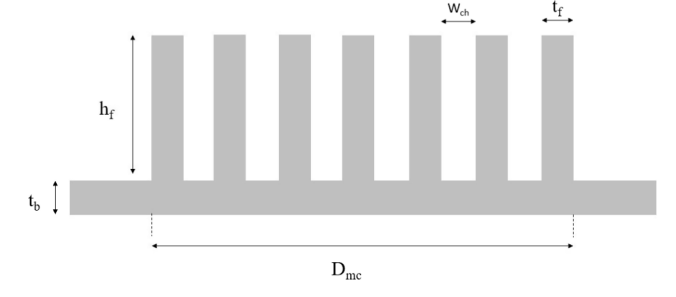


Fig. 5. Schematic diagram showing parameters of the heat sink.

 $\label{eq:table 1} \textbf{Table 1} \\ \textbf{Geometrical dimension of microchannel and pin fin array heat sink (L_p and W_g is the parameters of pin fin array heat sink in Fig. 10b).}$

t _b (mm)	h _f (mm)	W _{ch} (mm)	t _f (mm)	D_{mc} (mm)	L _p (mm)	W _g (mm)
3	3	0.1	0.1	26	1	1

previous work [35]. It was shown in Fig. 5 the schematic diagram and geometry parameters of the heat sink. D_{mc} stands for the diameter of circular area covered by microchannels. Table 1 shows the geometrical dimensions of the heat sink. In the experiment, the coolant entered heat sink from the inlet, impinged down to the microchannels and the heat

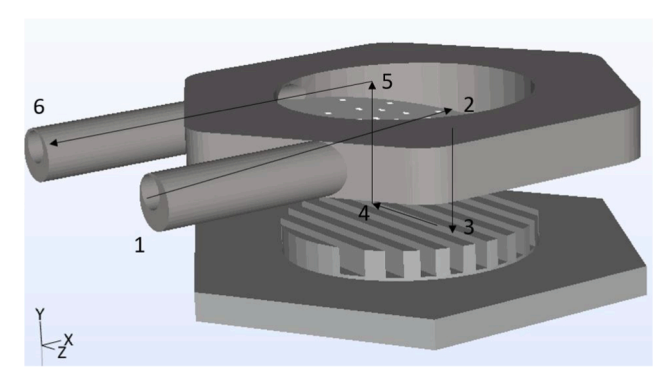


Fig. 6. Schematic showing heat sink design and flow direction (microchannel heat sink).

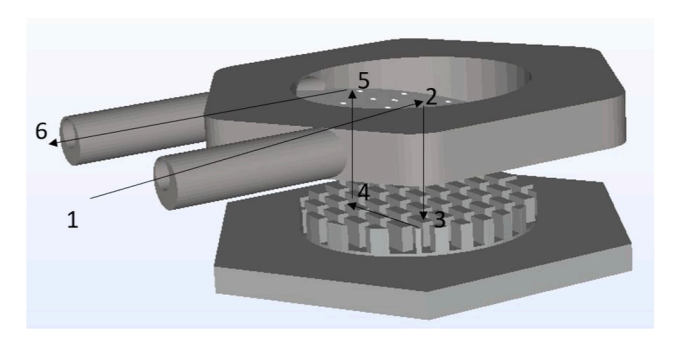


Fig. 7. Schematic showing heat sink design and flow direction (pin fin array heat sink).

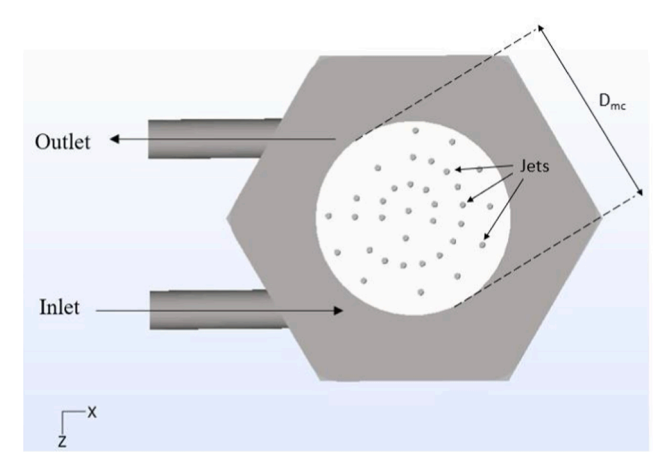


Fig. 8. Multi-jet distribution.

sink base through multiple jets, and then exited the heat sink at the outlet.

The Figs. 6–8 presented how the fins line up with the impinging jets and the multi-jets distribution. In this paper, three fin configurations were tested including microchannel fins, pin fin arrays and bare copper surface in Figs. 9a–9c. The original heat sink has microchannel fins. In order to obtain pin fins, the microchannel was cut into pin fin arrays using electrical discharge machining (EDM). There were 15 pin fin arrays which were numbered in Fig. 10a. Each individual pin fin in this arrangement had a width of 0.1 mm and a length of 1 mm. A picture of two adjacent pin fin arrays was captured by a stereo microscope in Fig. 10b. It can be observed in Fig. 10b that a gap $W_{\rm g}$ of 1 mm was created between each pin fins array using EDM. Two slots with a width of 0.76 mm and 0.76 mm deep was cut at the bottom of heat sink to



Fig. 9a. Microchannel.

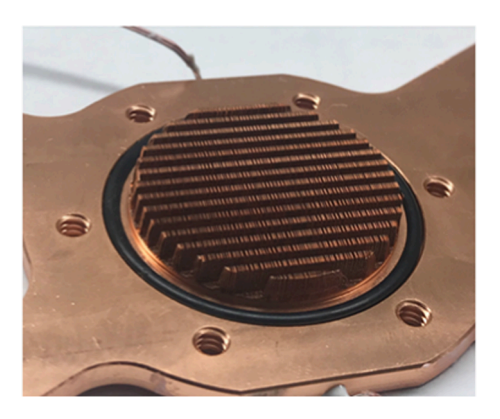


Fig. 9b. Pin fin arrays.



Fig. 9c. Bare copper surface.

accommodate T-type thermocouples in order to measure the heat sink's wall temperature (T_w) (Fig. 11).

2.3. Experimental procedures

The flow in the test loop was pumped through the coolant loop using a centrifugal pump. The required mass flow rate is regulated by the power supply connected to the pump. The coolant inlet temperature was controlled by using the chiller and the liquid—liquid heat exchanger. Two T-type thermocouples were installed at the inlet and outlet of heat sink in order to measure temperature before and after the coolant entered and exited the heat sink. The coolant enters the heat sink as single-phase liquid and leaves the heat sink as a two-phase mixture of liquid and vapor. The mixture entered the heat exchanger and was condensed to single-phase liquid. A differential pressure sensor was used to measure pressure drop through the heat sink. Two pressure

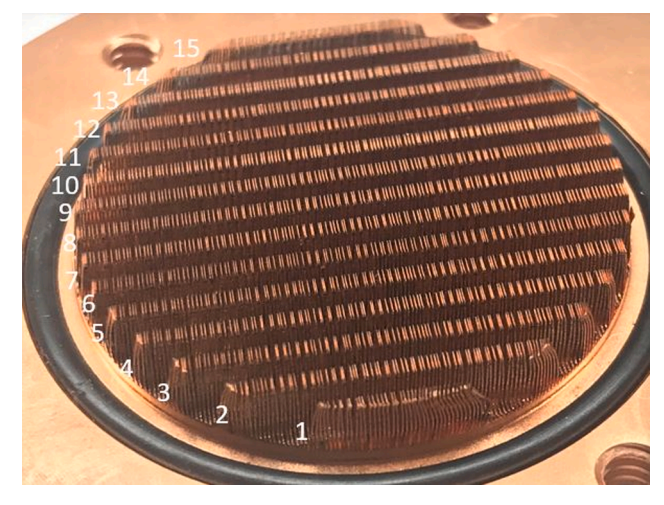


Fig. 10a. Pin fin array heat sink with 15 arrays in total.

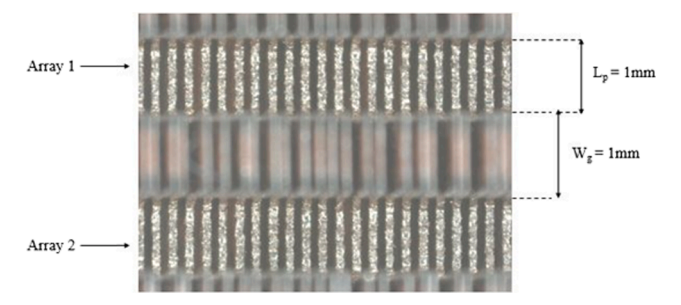


Fig. 10b. Microscope picture of two adjacent pin-fin arrays.

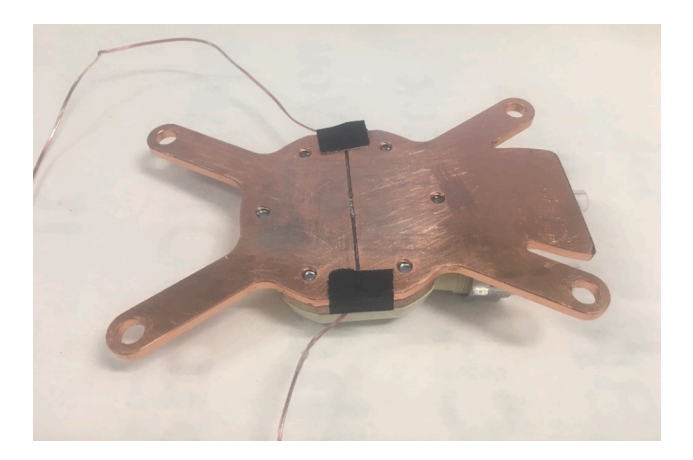


Fig. 11. Two slots at the bottom base of heat sink were machined for accommodating the two thermocouples for measuring the wall temperature.

transducers were installed at the inlet and outlet of heat sink in order to measure pressure at inlet and outlet. The outlet pressure was considered as saturation pressure and used to determine saturation temperature. The copper block is heated stepwise by the AC power supply. The time interval between each power step was controlled to ensure steady state conditions were maintained in the heat sink. All of the experimental data was acquired by the National Instrument acquisition system and compiled into an Excel file via a LABVIEW program. A vent valve at the reservoir was used for degassing and controlling the pressure inside the loop. Before gathering any data, the setup was maintained at desired temperature higher than room temperature. The air trapped inside the reservoir will move up to the liquid surface due to lower density of air.

Table 3Measurement Instruments and Uncertainty.

Instruments	Measurand	Uncertainty	DAQ Module
Pressure Gauges (Omega): PX309050A5V	P _{in} , P _{out}	$\pm 0.8~\mathrm{kPa}$	NI- USB- 6009
T-type Thermocouple: Laboratory Made	T _{in} , T _{out} , T _w	\pm 0.2 °C	NI 9219
Thermocouple (Omega): TJ36- CASS-116E-2-CC	Heat Flux Measurement	\pm 0.2 °C	NI 9219
Flow meter (Omega): FTB 313D	Flow Rate	\pm 6%	_
Differential pressure sensor (Omega) PX2300-10DI	Differential Pressure Drop	0.25 %	NI- USB- 6009

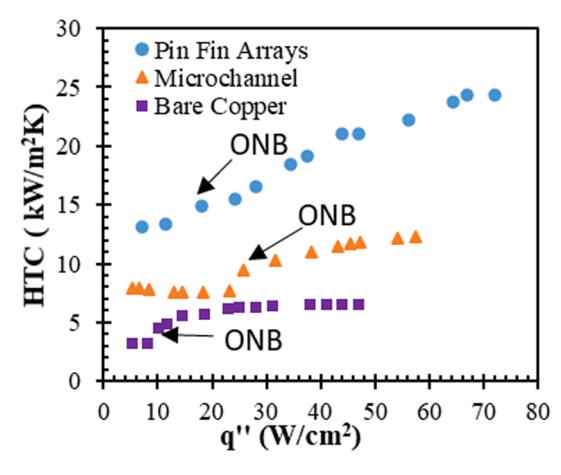


Fig. 12a. Comparison in heat transfer coefficient of pin fin array heat sink, microchannel heat sink and bare copper surface heat sink. $T_{in}=36\,^{\circ}C$, flow rate 1 L/min.

The vent valve was opened by a little so that the air can be removed. In addition, by opening the vent valve by a little, the pressure inside the loop can be reduced to the desired pressure for gathering data.

3. Heat loss and uncertainty analysis

Experiment was performed at low heat flux and single-phase state to determine the heat losses via measuring the difference between sensible heat absorbed by the coolant and the measured electrical power input. Heat loss was less than 5% in all data points. The measurement uncertainties of each instrument in the experimental test facility are listed

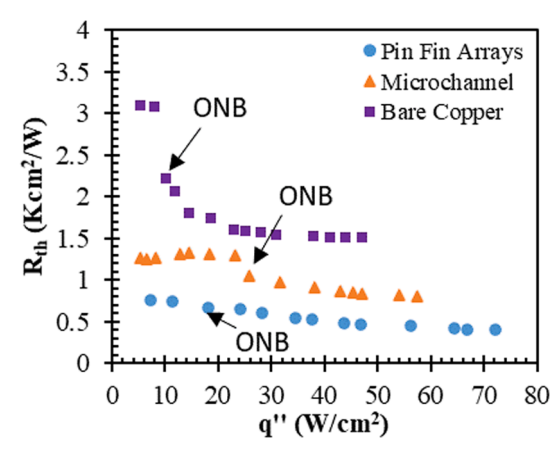


Fig. 12b. Comparison in specific thermal resistance of pin fin array heat sink, microchannel heat sink and bare copper surface heat sink, $T_{\rm in}=36$ °C, flow rate 1 L/min.

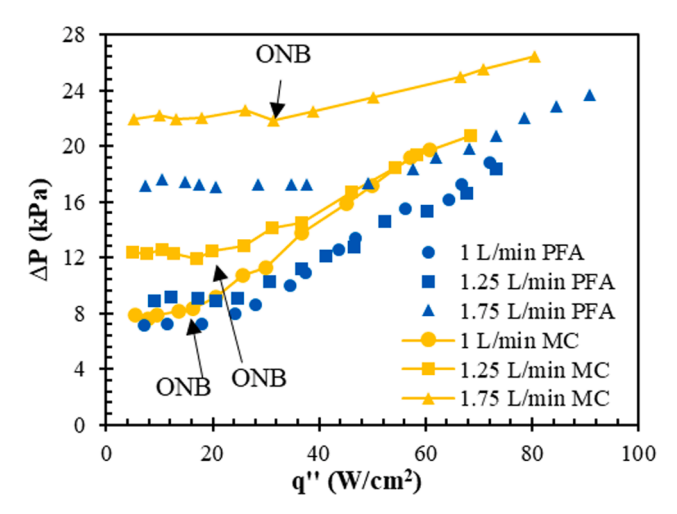


Fig. 13a. Comparison in pressure drop of pin fin array (PFA) heat sink and microchannel (MC) heat sink with variation in flow rate.

in Table 3. The uncertainty of thermal resistance was calculated using root sum square method [40]. The maximum uncertainties in thermal resistance, pressure drop and heat transfer coefficient occur at low heat fluxes (and low chip temperatures) and generally decrease with increasing heat flux. Uncertainty of thermal resistance was reduced from 13 % to 2 % when heat flux was increased from 5 W/cm² to 81 W/cm².

4. Results and discussions

4.1. Comparison of three fin configurations

Three different fin configurations were tested in this paper including original microchannel, pin fin array and bare copper surface (no fin). Figs. 12a and 12b shows heat transfer coefficient and thermal resistance variation with heat flux for three fin configurations. The specific thermal resistance was defined by:

$$R_{th} = \frac{A(T_w - T_{in})}{O} \tag{1}$$

where T_b is the base temperature, T_{in} is the coolant inlet temperature, Q is the power absorbed by the coolant and A is surface area covered by microchannels. It was observed in Fig. 12b that pin fin array heat sink has the better thermal performance than microchannel heat sink and bare surface heat sink. With pin fins array heat sink, specific thermal resistance was reduced to 0.41 Kcm²/W which is 51 % lower than the specific thermal resistance of the original microchannel heat sink. At the same heat flux of 60 W/cm^2 , heat transfer coefficient of pin fin array was around $22 \text{ kW/m}^2\text{K}$ as compared to $12 \text{ kW/m}^2\text{K}$ of microchannel heat sink. The heat transfer coefficient of the heat sink was calculated via:

$$h = \frac{Q}{A(T_W - T_{in})} \tag{2}$$

where Q is the input power (W), A is the area covered by microchannel (m²), T_w is wall temperature (°C) and T_{in} is the inlet temperature (°C). The heat transfer coefficient of pin fin arrays heat sink improved significantly as compared to the one of microchannel heat sink. In this specific heat sink design, the microchannel width is 100 μm which is very small as compared to channel height of 3000 μm . Due to the small width of the channel in the microchannel heat sink, the coolant that impinged down from the multi-jets was unable to penetrate through to the base and could not remove heat flux very well. When the microchannels was cut into pin fin arrays with a big gap of 1 mm between adjacent arrays, coolant was able to penetrate through to the base and remove heat flux more effectively. Therefore, the thermal performance

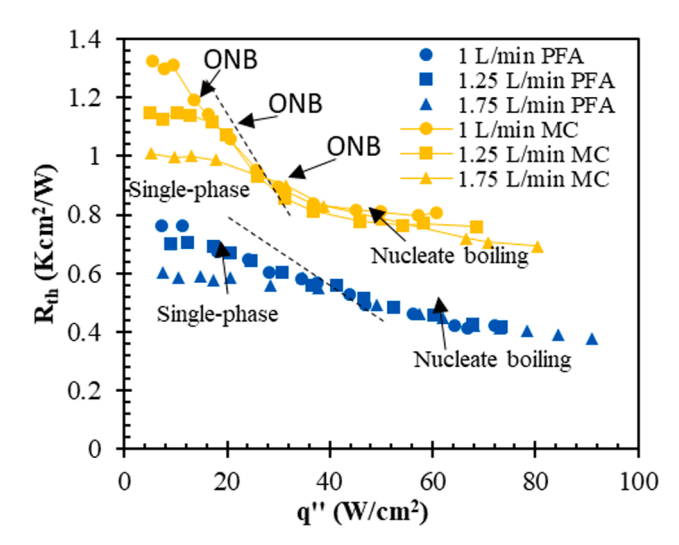


Fig. 13b. Comparison in specific thermal resistance of pin fin array (PFA) heat sink and microchannel (MC) heat sink with variation in flow rate.

Table 4 Experimental data for the case of pin fin array heat sink at flow rate 1 LPM, $T_{\rm in}$ 36 $^{\circ}\text{C}.$

q" (W/ cm ²)	T _{in} (°C)	Flow rate (L/ min)	T _b (°C)	R _{th} (Kcm ² / W)	ΔP (Kpa)
7.2	36.1	1	41.3	0.76	7.1
11.4	36.4	1	44.5	0.75	7.2
18	36.8	1	48.5	0.67	7.2
24.2	36.1	1	51.3	0.65	8.0
28.1	36.0	1	52.5	0.60	8.6
34.5	36.3	1	54.6	0.54	10.0
37.5	36.1	1	55.2	0.52	10.9
43.8	36.3	1	56.6	0.48	12.6
46.8	36.0	1	57.7	0.48	13.4
56.1	36.3	1	60.9	0.45	15.5
64.3	36.2	1	62.7	0.42	16.2
66.8	36.7	1	63.5	0.41	17.2
72.1	36.6	1	66.5	0.42	18.8

of the pin fin array heat sink was better than the original microchannel heat sink. Of the three configurations, the bare copper surface heat sink had the poorest thermal performance, which was attributed to the reduced contact area between the copper surface and the coolant. In comparison with our previous work [35], where the impact of microchannel fin height was performed, cutting of microchannel to pin fin arrays even shows higher enhancement with 51% increase in heat transfer coefficient; meanwhile, variation in microchannel fin height can lead to only 46% enhancement in heat transfer coefficient as compared to original heat sink.

4.2. Comparison of pin fin array and microchannel fin

Comparison between thermal–hydraulic performance of microchannel and pin fin arrays with variation of flow rate was presented in Figs. 13a and 13b. The experiment was conducted at different flow rates: 1 L/min, 1.25 L/min, and 1.75 L/min. Pin fin arrays heat sink performs better not only in thermal resistance but also in pressure drop. At the same conditions, which were a flow rate of 1 L/min and a heat flux of 71 W/cm², the pressure drop of the pin fin array heat sink was 18 % lower than that of the heat sink. Table 4 shows experimental data for the case of pin fin array heat sink at flow rate 1 LPM, $T_{\rm in}$ of 36 °C. The onset of nucleate boiling was delayed when flow rate was increased from 1 L/min to 1.75 L/min. It was observed in Figs. 13a and 13b that for pin fin array heat sink shown in blue, the onset of nucleate boiling happened at heat flux 18 W/cm² for flow rate 1 L/min, 24 W/cm² for flow rate 1.25

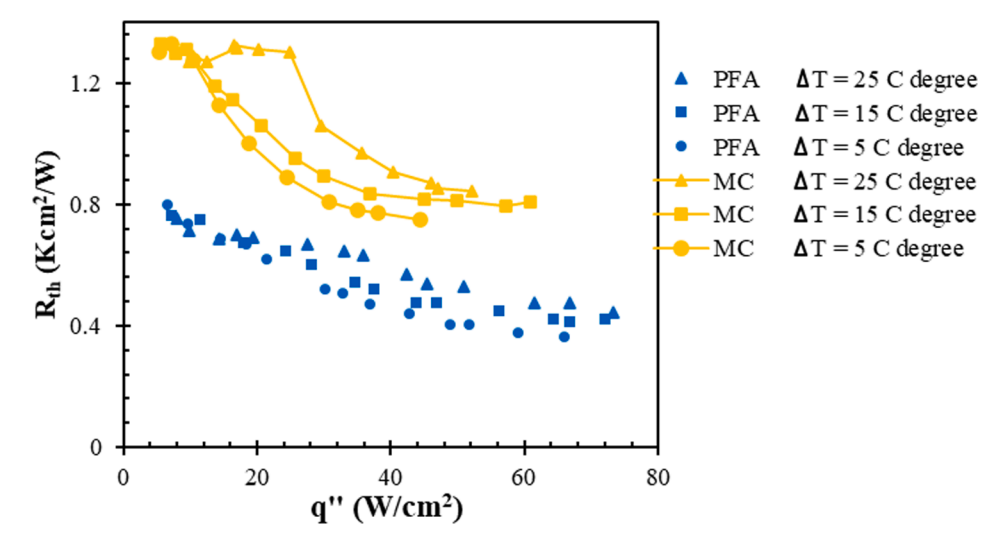


Fig. 14. Comparison in specific thermal resistance of pin fin array (PFA) heat sink and microchannel (MC) heat sink with variation in subcooling (5 °C < ΔT < 25 °C), $T_{sat} = 51$ °C, flow rate 1 L/min.

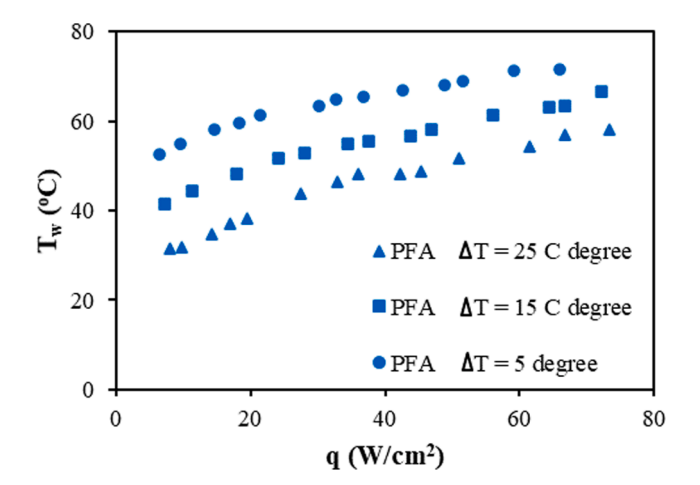


Fig. 15a. Effects of subcooling on wall temperature of the pin fin array (PFA) heat sink at the same flow rate 1 L/min (5 $^{\circ}C<\Delta T<25$ $^{\circ}C).$

L/min and 48 W/cm² for flow rate 1.75 L/min. Fig. 13b shows that there were two heat transfer mechanisms when the heat flux was varied from 0 to 93 W/cm². At lower heat fluxes, single-phase convection is dominant and thermal resistance reduces considerably with flow rate. On the other hand, at higher heat fluxes, the nucleate boiling mechanism becomes dominant and thermal resistance is weekly dependent on flow rate. At high heat fluxes the flow rate could be reduced to lower the pressure drop while maintaining a similar thermal performance. However, close attention should be paid to the critical heat flux value because critical heat flux will decrease when the flow rate is reduced. The thermal resistance in nucleate boiling mechanism decreases with increasing heat flux. The increasing trend of thermal performance with increasing heat flux can help in cooling of hot spots.

Fig. 14 presents a comparison of the thermal–hydraulic performance of the microchannel to the pin fin array heat sink with variation in the subcooling and the same flow rate (1 L/min). For the pin fin array heat sink, the thermal resistance was lower with less subcooling. At the same heat flux of 44 W/cm², the thermal resistance was 0.48 Kcm²/W when the degree of subcooling was 5 °C and 0.61 Kcm²/W when the degree of subcooling was 15 °C. The lower thermal resistance at a lower degree of subcooling was attributed to the higher vapor quality that was being generated when the coolant was pumped into the heat sink at a temperature closer to the saturation temperature. With more heat flux being

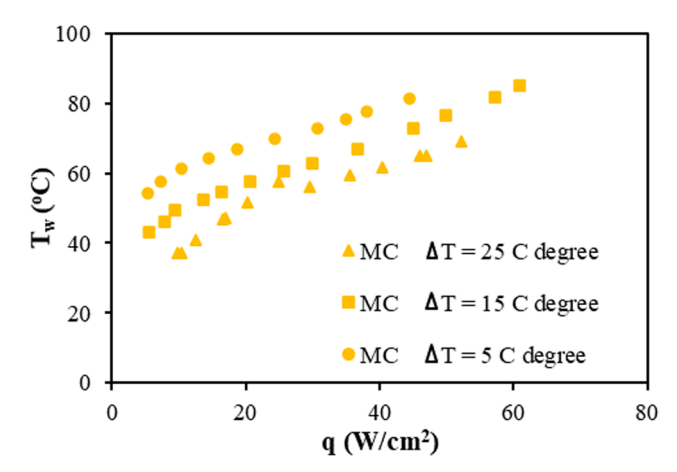


Fig. 15b. Effects of subcooling on wall temperature of the original microchannel (MC) heat sink at the same flow rate 1 L/min (5 $^{\circ}$ C < ΔT < 25 $^{\circ}$ C).

removed by latent heat, the heat transfer coefficient was higher.

Effects of subcooling on the wall temperature of the pin fin array heat sink and original microchannel heat sink were presented in Figs. 15a and 15b, respectively. It was observed that the wall temperature decreased with more subcooling. For the pin fin array heat sink at the same heat flux of 65 W/cm², the wall temperature was 55 °C when the degree of subcooling was 25 °C and 71 °C when the degree of subcooling was 5 °C. While thermal resistance was lower with less subcooling, the wall temperature was higher with less subcooling because the coolant inlet temperature increased. The wall temperature of pin fin array heat sink was significantly lower than original microchannel heat sink. At the same heat flux of 64 W/cm² when the degree of subcooling was 15 °C, the wall temperature was 63 °C for the pin fin array heat sink and 85 °C for the original microchannel heat sink.

4.3. Comparison to existing correlations

The experimental results obtained in this study were compared to several predictive correlations proposed in the literature. Of the many predictive correlations for boiling heat transfer proposed in the literature, those by Rhosenow [41] and Cooper [42] are widely used for predicting nucleate pool boiling heat transfer coefficients. Rohsenow [41] has developed the first and most widely used correlation for nucleate boiling. Data for nucleate boiling of a liquid on a clean surface

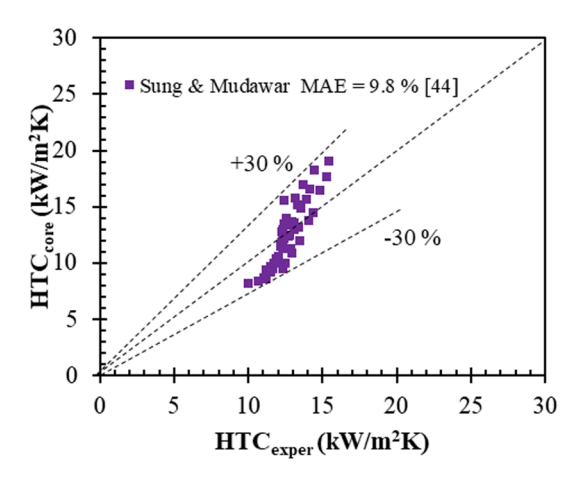


Fig. 16a. Comparison of experimental data with existing correlation (Sung & Mudawar [44]) for the case of microchannel.

can be correlated by an equation of the form:

$$\frac{Q}{A} = \mu_{L} h_{fg} \left[\frac{g(\rho_{L} - \rho_{v})}{\sigma} \right]^{1/2} \left[\frac{C_{pL}(T_{W} - T_{sat})}{C_{sf} h_{fg} P r_{L}^{n}} \right]^{3}$$
(3)

where C_{pL} is the specific heat of the liquid. C_{sf} is a function of the particular heating surface-fluid combination and equals to 0.015 for copper and Novec/HFE 7000 surface fluid combination. σ is the surface tension of the liquid–vapor interface. The variable n depends on the surface fluid combination and typically has a value of 1.0 or 1.7.

Cooper [42] developed a correlation for calculation of heat transfer coefficient in nucleate pool boiling mechanism. The two-phase heat transfer coefficient contribution in Cooper's study is given by:

$$h_{2\phi} = 55P_r^{0.12 - 0.4343ln(R_p)} (-0.4343ln(P_r))^{-0.55} M^{-0.5} q'^{0.67}$$
(4)

where P_r is the reduced pressure (P_{out}/P_{crit}), P_{out} is the outlet pressure of the heat sink, P_{crit} is the critical pressure, M is the molar mass of the coolant, R_p is the roughness in microns.

Flow boiling is characterized by simultaneous contributing factors from nucleate boiling and forced convection. Buchanan and Shedd [43] introduced a simple asymptotic matching principle that considers contribution of both forced convection factor $h_{1\phi}$ and the nucleate boiling factor $h_{2\phi}$ given in Eq. (4). The matching has the form $h_{tot}=(h_{1\phi}^z+h_{2\phi}^z)^{1/z}$. Here, the asymptotic matching parameter, z, was set to 5. The single-phase heat transfer coefficient contribution $h_{1\phi}$ is given by:

$$h_{1\phi} = \frac{Nu_{d_n}k_l}{d_n} \tag{5}$$

where $d_n = 1$ mm is the jet diameter, k_l is the liquid thermal conductivity and Nu_{d_n} is the Nusselt number given by the equation:

$$Nu_{d_n} = 0.45 \left(\frac{S}{d_n}\right)^{2/5} \left(\frac{L}{d_n}\right)^{-1/2} Re_{d_n}^{2/3} Pr_l^{1/3}$$
 (6)

where S is the jet spacing, d_n is jet diameter, L is the distance between the jet and the base, Pr_l is the Prandtl number of the liquid and Re_{d_n} is the Reynolds number based on jet diameter and is given by:

$$Re_{d_n} = \frac{\rho_l u d_n}{\mu_l} \tag{7}$$

where ρ_1 is the liquid density, u is the liquid velocity and μ_1 is the liquid viscosity.

In a study by Sung and Mudawar [44], nucleate boiling data for a hybrid micro-channel/micro-circular-jet- impingement module were correlated using heat flux and subcooling. The equation for predicting

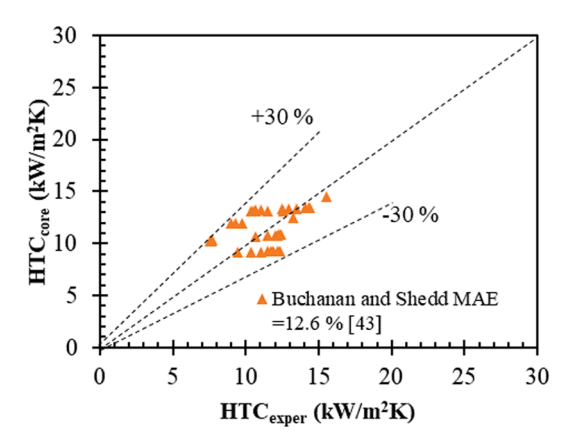


Fig. 16b. Comparison of experimental data with existing correlation (Buchanan & Shedd [43]) for the case of microchannel.

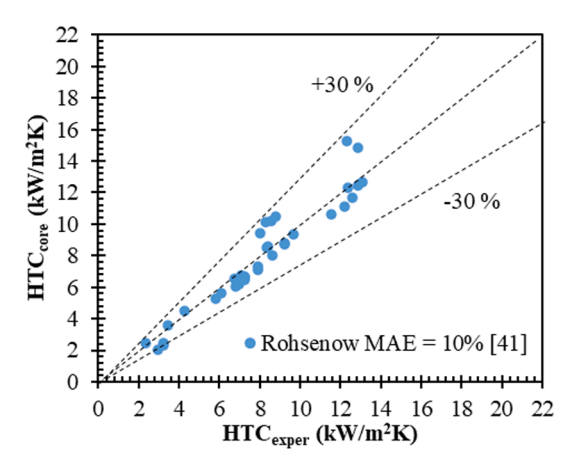


Fig. 17a. Comparison of experimental data with existing correlation (Rohsenow [41]) for the case of bare copper surface.

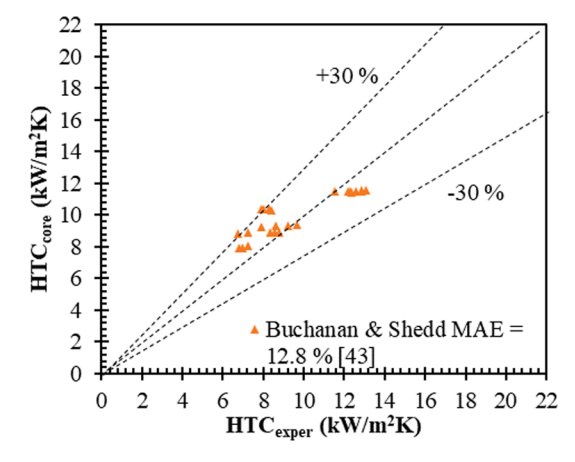


Fig. 17b. Comparison of experimental data with existing correlation (Buchanan & Shedd [43]) for the case of bare copper surface.

the heat transfer coefficient is given by:

$$h = \frac{q'}{\left(\frac{q''}{C}\right)^{1/n} + \Delta T_{sub}} \tag{8}$$

where q" is the heat flux (W/m^2) and ΔT_{sub} is the subcooling (°C). The empirical constants n and C were obtained by least-square's fit and are equal to 43.88 and 0.33, respectively. The comparison between

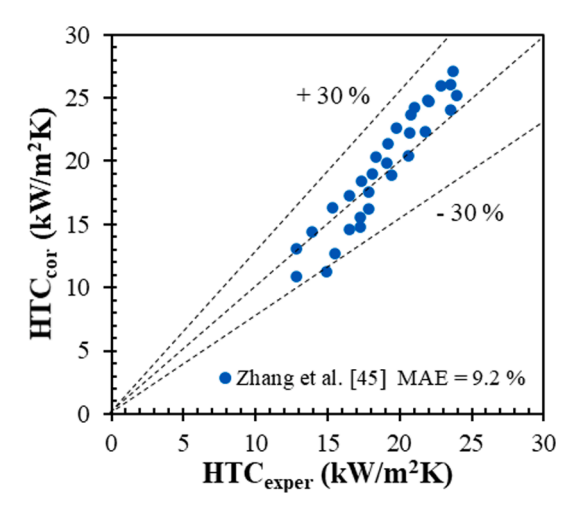


Fig. 18. Comparison of experimental data with an existing correlation [45] for the case of pin fin array.

experimental data and correlations mentioned above [41,43,44] are illustrated in Figs. 16a and 16b, Figs. 17a and 17b, and Fig. 18.

A comparison of experimental data with existing correlations for microchannel fins was presented in Figs. 16a and 16b. Among the correlations considered, Sung and Mudawar's nucleate boiling correlation [44] best predicts the experimental results for the original microchannel heat sink in this study. The mean absolute error (MAE) in the prediction from Sung and Mudawar's correlation was 9.8 % (Fig. 16a), while for Buchanan and Shedd's correlation [43] it was 12.6 % (Fig. 16b). Sung and Mudawar developed a correlation for a micro-channel/microcircular-jet- impingement heat sink which is similar to the geometry of the heat sink in present study; therefore, the Sung and Mudawar's correlation best predicts experimental data.

A comparison of experimental data with existing correlations for the bare copper surface configuration was presented in Figs. 17a and 17b. Of the correlations considered, Rohsenow's correlation, which was developed for a bare surface, best predicted the experimental data for the bare copper surface configuration in this study. The MAE in its prediction was 10%, which was considered very good (Fig. 17a). Although Buchanan and Shedd's correlation [43] was also developed for a bare surface, it generally overpredicted the experimental data for the bare copper surface configuration in this study with a MAE of 12.8 % (Fig. 17b). Since Sung and Mudawar's correlation was developed for a microchannel heat sink, it was not used for comparison with the bare copper surface configuration in this study

A comparison of the experimental data for the pin fin array configuration to an existing correlation is presented in Fig. 18. Zhang et al. [45] developed a heat transfer correlation for jet impingement boiling on micro-pin-finned surface. Two-phase Nusselt number is given by:

$$Nu = KPr^{a}Re^{b}Bo^{c}\left(0.7605 + 0.215\frac{A}{A_{s}} + 18.27\frac{D_{h}}{L_{h}}\right)^{n}$$
(9)

where $Bo = \frac{q}{\rho V_i h_{fg}}$ is the boiling number, A is heat transfer area of micro pin-fins, A_s is the heat transfer area of the smooth surface, D_h is the hydraulic diameter of the inter-connected channel formed by micro-pin-fins, L_h is cross-flow distance of each nozzle, ρ is the density of the coolant (kg/m^3) , V_j is the volumetric flow rate (m^3/s) , h_{fg} is the latent heat of the coolant (J/kg). Here, K=3.977, a=0.4, b=0.445, c=0.631, n=0.966 for the micro-pin-fins. In the original paper of Zhang [45], b was equal to 0.767 instead of 0.445. It should be noted that the dielectric coolant used in Zhang's paper (FC 72) was different than the one in the present study (Novec/HFE 7000). Additionally, the geometry parameters were different for each study. Therefore, some of the coefficients in Zhang's correlation were modified to assure good prediction

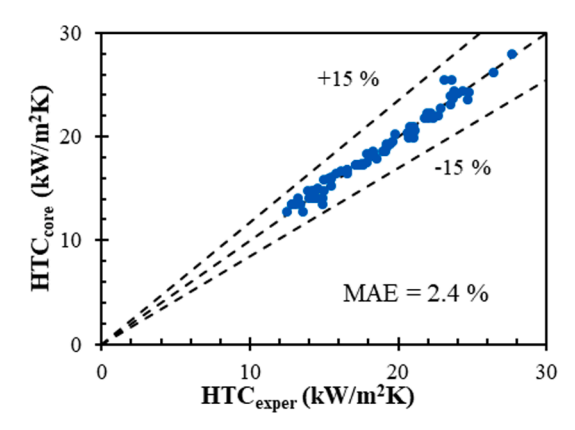


Fig. 19. Comparison of experimental data and proposed correlation for heat transfer coefficient. Subcooling varies from 5 to 25C degree, and flow rate varies from 1 to 1.75 L/min, heat fluxes vary from 5 to 91 W/cm².

of the experimental data in the current study. Fig. 18 shows that there was good agreement between the experimental data and the correlation, with a MAE of 9.2 %. Of the data, 93.3 % and 96.7 % were predicted within ± 20 % and ± 30 %, respectively.

4.4. New predicting method

At the time of this study, correlations that predicted the heat transfer coefficient of pin fin heat sink were notably rare in the literature and further elaborative experimental efforts were required. The current study proposes a new empirical model based on a full factorial design that will predict experimental data for the heat transfer coefficient of the pin fin array configuration. Using the commercial software Minitab, the regression function of the correlation was developed from 82 experimental data points in both single-phase and two-phase regime and can be applied for the entire range of heat fluxes (single phase, nucleate boiling). Nusselt number of single-phase contribution ($Nu_{1\phi}$) and evaporation contribution ($Nu_{2\phi}$) are defined by:

$$Nu_{10} = 128.6 - 24.70 + 0.0335Re \tag{10}$$

$$Nu_{2\varphi} = 180.4 + 36\alpha - 1.10 - 0.012Re + 29.30\alpha - 0.0058\alpha Re$$
 (11)

where Re is Reynolds number, α and θ are nondimensional forms of heat flux, and inlet temperature, respectively. The dimensionless variables θ , α and Re were defined by following:

$$Re = \frac{\rho u d_n}{\mu}, \ \alpha = 10^{-2} \times \left(\frac{q' d_n}{k_l T_o}\right), \ \theta = \frac{T_{in} - T_o}{T_{sat} - T_o}$$
 (12)

where T_{in} (°C) is inlet temperature, T_{o} is ambient temperature (20 °C), T_{sat} (°C) is saturation temperature, q" is heat flux (w/m²), d_{n} (m) is nozzle (jet) diameter and k_{l} is liquid thermal conductivity (W/m.K).

Nusselt number in single-phase regime and two-phase regime are calculated as following:

In single-phase regime: $N_{total} = Nu_{1\varphi}$

In two-phase regime: $Nu_{total} = (Nu_{1\omega}^z + Nu_{2\omega}^z)^{1/z}, (z = 5)$

In nondimensional form, Nusselt number is defined by: $Nu = \frac{hd_n}{k}$.

Therefore, heat transfer coefficient was calculated from Nusselt number: $h = \frac{k_l N u}{d}$

Fig. 19 shows that the new correlation predicted the experimental data with a MAE of 2.4 %, which is considered very good. In the current study, the pin fins did not vary in dimension. Thus, the geometrical parameters of the pin fin were not included in the regression function. In the future work, variations in dimension of the fin can be taken into account and the regression function may include some geometry parameters such as hydraulic diameter, heat transfer area of the pin fin, the

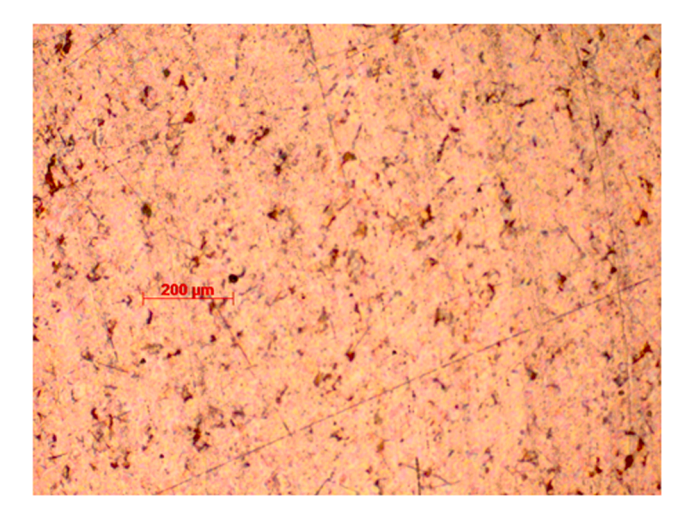
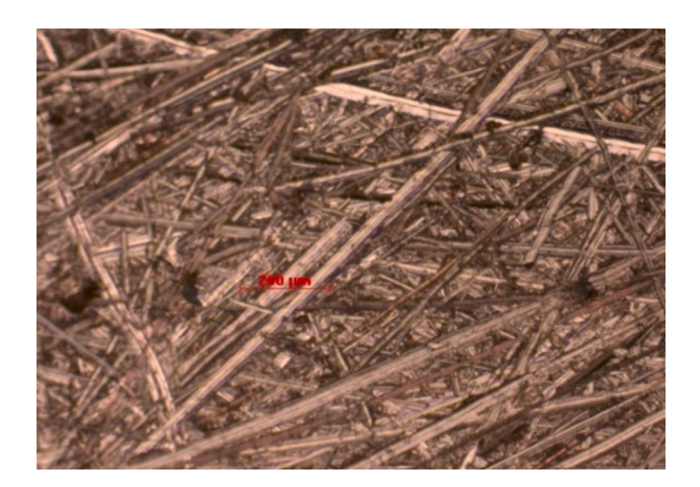


Fig. 20a. Optical microscope picture of the bare copper surface without applying sandpaper.



 $\textbf{Fig. 20b.} \ \ \textbf{Optical microscope picture of the bare copper surface with surface modification using sandpaper.}$

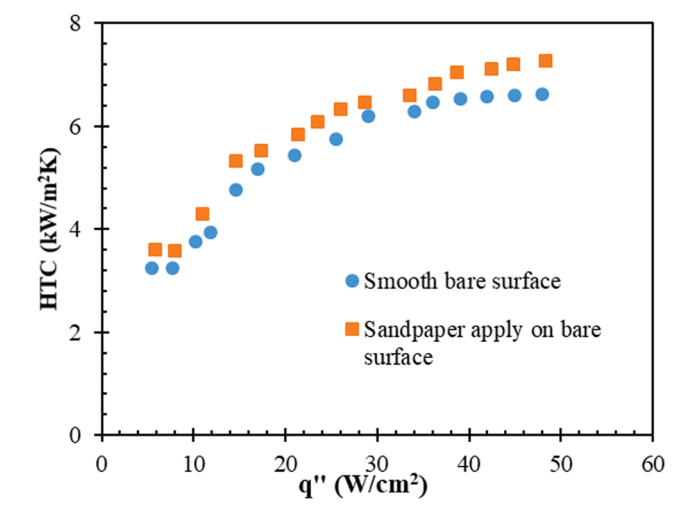


Fig. 21. Heat transfer coefficient of the bare surface heat sink in the case of smooth surface and enhanced surface using sandpaper.

gap between two adjacent pin fin arrays W_o, fin height h_f.

4.5. Effects of surface roughness

One drawback of cooling via boiling is the ineffective heat transfer on very smooth surfaces, like the untreated copper surface. Higher surface roughness can lead to a higher nucleation site density, which enhances boiling heat transfer and makes the spatial temperature distribution more uniform. Considering this, 120-grit sandpaper was used to modify the bare copper surface in this study by increasing its surface roughness. Figs. 20a and 20b show microscopic pictures of the original bare copper surface and the modified copper surface, the latter which has a visible increase of surface roughness

Fig. 21 compares the heat transfer coefficient of the smooth bare copper surface to the modified copper surface. Although the heat transfer coefficient of the modified copper surface was slightly higher than that of the bare copper surface, the thermal performance did not greatly improve. At the heat flux of 48 W/cm², the heat transfer coefficient of the modified copper surface was 7.3 kW/m²K which is 9 % higher than the smooth surface. This value of 9% is higher than the uncertainty of 2%; therefore, the increase in heat transfer coefficient is significant. This improvement is much lower than that obtained by cutting the microchannel into pin fin arrays (Section 4.1), which increased thermal performance by 51 %.

5. Conclusions

In this study, we investigate the thermal–hydraulic performance of a two-phase multi-jet impingement heat sink with three different fin geometries including microchannel, pin fin arrays and bare copper surface. The primary findings of this study are as follows:

- The heat transfer coefficient increases with heat flux over the range tested for all three fin geometries. As compared to microchannel heat sink, pin fin arrays heat sink shows 51 % improvement in thermal performance and 18 % lower in pressure drop. The bare copper surface has the lowest thermal performance due to limited liquid—solid contact surface area.
- The experimental results were compared with three different correlations. The Sung and Mudawar [44] nucleate boiling correlation provided a good prediction of the experimental heat transfer coefficient of the original microchannel heat sink configuration, with a mean absolute error (MAE) of 9.8 %. The Rhosenow [41] correlation provided a good prediction of the experimental heat transfer coefficient of the bare copper surface configuration, with an MAE of 10 %. The Zhang [45] correlation provided a good prediction of the experimental data of the pin fin array configuration, with an MAE of 9.2 %.
- A new correlation was developed that provided a good prediction of the experimental data from the 82 trials of this study, with a MAE of 2.4 %. In this correlation, the Nusselt number was a function of the Reynolds number, heat flux, and inlet temperature.
- The effects of surface enhancement on the performance of the bare copper surface were also examined. Scuffing the surface with sandpaper increased the heat transfer coefficient by ~9 %.

Declaration of Competing Interest

The authors declare that they have no known competing financial interests or personal relationships that could have appeared to influence the work reported in this paper.

Acknowledgement

The research reported herein was supported by a grant from the National Science Foundation Industry/University Cooperative Research

Center Award No. IIP-1738793 and the Semiconductor Research Corporation (SRC). The author would like to thank Mr. Eugene Mazza from Mechanical Specialties in Binghamton, NY for his help with machining the heat sink.

References

- N. Jones, How to stop data centres from gobbling up the world's electricity, Nature 561 (7722) (2018) 163–166, https://doi.org/10.1038/d41586-018-06610-y.
- [2] S.V. Garimella, T. Persoons, J. Weibel, L.T. Yeh, Technological drivers in data centers and telecom systems: Multiscale thermal, electrical, and energy management, Appl. Energy 107 (2013) 66–80, https://doi.org/10.1016/j. apenergy.2013.02.047.
- [3] Arman Shehabi, S. J. Smith, D. A. Sartor, R. Brown, M. Herrlin, J. Koomey, E. Masanet, N. Horner, I. L. Azevedo, W. Lintner, "United States Data Center Energy Usage Report | Energy Technologies Area," no. June, 2016, pp. 65 [Online]. Available: https://eta.lbl.gov/publications/united-states-data-center-energy.
- [4] R. Schmidt, Packaging of New Servers, Energy Efficiency Aspects, in: 1st Berkeley Symposium on Energy Efficient Electronics., Aug. 9–12, 2009.
- [5] Michael J. Ellsworth Jr., Comparing Liquid Coolants From Both A Thermal And Hydraulic Perspective, ElectronicsCooling 12 (2) (2006).
- [6] Tianyi Gao, Shuai Shao, Yan Cui, Bryan Espiritti, Charles Ingalz, Hu Tang, Ali Heydari, A Study of Direct Liquid Cooling for High-Density Chips and Accelerators, in: Proceedings of the 16th InterSociety Conference on Thermal and Thermomechanical Phenomena in Electronic Systems, ITherm 2017, 2017, pp. 565–73. http://dx.doi.10.1109/ITHERM.2017.7992537.
- [7] C. Nadjahi, H. Louahlia, S. Lemasson, A Review of Thermal Management and Innovative Cooling Strategies for Data Center, Sustainable Comput. Inf. Syst. 19 (May) (2018) 14–28, https://doi.org/10.1016/j.suscom.2018.05.002.
- [8] A.C. Kheirabadi, D. Groulx, Experimental evaluation of a thermal contact liquid cooling system for server electronics, Appl. Therm. Eng. 129 (2018) 1010–1025, https://doi.org/10.1016/j.applthermaleng.2017.10.098.
- [9] P. Shahi, S. Agarwal, S. Saini, A. Niazmand, P. Bansode, and D. Agonafer, CFD Analysis on Liquid Cooled Cold Plate Using Copper Nanoparticles, Oct. 27, 2020. http://dx.doi.10.1115/IPACK2020-2592.
- [10] K. Zhang, Y. Zhang, J. Liu, X. Niu, Recent Advancements on Thermal Management and Evaluation for Data Centers, Appl. Therm. Eng. 142 (April) (2018) 215–231, https://doi.org/10.1016/j.applthermaleng.2018.07.004.
- [11] Y. Hadad, N. Fallahtafti, L. Choobineh, C.H. Hoang, V. Radmard, P.R. Chiarot, B. Sammakia, Performance Analysis and Shape Optimization of an Impingement Microchannel Cold Plate, IEEE Trans. Compon. Packag. Manuf. Technol. 10 (8) (2020) 1304–1319, https://doi.org/10.1109/tcpmt.2020.3005824.
- [12] V. Radmard, Y. Hadad, A. Azizi, S. Rangarajan, C.H. Hoang, C. Arvin, K. Sikka, S.N. Schiffres, B. Sammakia, Direct Micro-Pin Jet Impingement Cooling for High Heat Flux Applications, in: 2020 36th Semiconductor Thermal Measurement, Modeling & Management Symposium (SEMI-THERM), 2020, pp. 1–9. http://dx.doi.10.239 19/SEMI-THERM50369, 2020, 9142864.
- [13] S.I. Guggari, Analysis of Thermal Performance Metrics-Application to CPU Cooling in HPC Servers, IEEE Trans. Components, Packag. Manuf. Technol. (2020) 1, https://doi.org/10.1109/TCPMT.2020.3029940.
- [14] A.C. Kheirabadi, D. Groulx, Cooling of server electronics: A design review of existing technology, Appl. Therm. Eng. 105 (2016) (2016) 622–638, https://doi. org/10.1016/j.applthermaleng.2016.03.056.
- [15] B. Rimbault, C.T. Nguyen, N. Galanis, Experimental investigation of CuO-water nanofluid flow and heat transfer inside a microchannel heat sink, Int. J. Therm. Sci. 84 (2014) 275–292, https://doi.org/10.1016/j.ijthermalsci.2014.05.025.
- [16] M.M. Ohadi, S.V. Dessiatoun, K. Choo, M. Pecht, J.V. Lawler, A Comparison Analysis of Air, Liquid, and Two-Phase Cooling of Data Centers, in: 2012 28th Annual IEEE Semiconductor Thermal Measurement and Management Symposium (SEMI-THERM), 2012, pp. 58–63. http://dx.doi.10.1109/STHERM.2012.6188826.
- [17] M. Law, P.S. Lee, A Comparative Study of Experimental Flow Boiling Heat Transfer and Pressure Characteristics in Straight- and Oblique-Finned Microchannels, Int. J. Heat Mass Transf. 85 (2015) 797–810, https://doi.org/10.1016/j. ijheatmasstransfer.2015.01.137.
- [18] S. Zhang, W. Yuan, Y. Tang, J. Chen, Z. Li, Enhanced Flow Boiling in an Interconnected Microchannel Net at Different Inlet Subcooling, Appl. Therm. Eng. 104 (2016) 659–667, https://doi.org/10.1016/j.applthermaleng.2016.05.117.
- [19] W. Wan, D. Deng, Q. Huang, T. Zeng, Y. Huang, Experimental Study and Optimization of Pin Fin Shapes in Flow Boiling of Micro Pin Fin Heat Sinks, Appl. Therm. Eng. 114 (2017) 436–449, https://doi.org/10.1016/j. applthermaleng.2016.11.182.
- [20] D.F. Sempértegui-Tapia, G. Ribatski, The effect of the cross-sectional geometry on saturated flow boilling heat transfer in horizontal micro-scale channels, Exp. Therm. Fluid Sci. 89 (2017) 98–109, https://doi.org/10.1016/j. exothermflusci.2017.08.001.
- [21] T. Harirchian, S.V. Garimella, Microchannel Size Effects on Local Flow Boiling Heat Transfer to a Dielectric Fluid, Int. J. Heat Mass Transf. 51 (15–16) (2008) 3724–3735, https://doi.org/10.1016/j.ijheatmasstransfer.2008.03.013.

- [22] D.C. Deisenroth, A. Bar-Cohen, M. Ohadi, Geometry Effects on Two-Phase Flow Regimes in a Diabatic Manifolded Microgap Channel (2017), https://doi.org/ 10.1115/IPACK2017-74287.
- [23] R. Mandel, A. Shooshtari, M. Ohadi, Effect of manifold flow configuration on twophase ultra-high flux cooling, Numer. Heat Transf. Part A Appl. 74 (2018) 1425–1442, https://doi.org/10.1080/10407782.2018.1538297.
- [24] K.W. Jung, C.R. Kharangate, H. Lee, J. Palko, F. Zhou, M. Asheghi, E.M. Dede, K.E. Goodson, Microchannel cooling strategies for high heat flux (1 kW/cm2) power electronic applications, in: 2017 16th IEEE Intersoc. Conf. Therm. Thermomechanical Phenom. Electron. Syst., 2017, pp. 98–104. http://dx.doi.10.1109/ITHERM.2017.7992457.
- [25] G. Hedau, R. Raj, S.K. Saha, Effect of outlet plenum design on flow boiling heat transfer in microchannel heat sinks, Therm. Sci. Eng. Prog. 23 (2021), 100868, https://doi.org/10.1016/j.tsep.2021.100868.
- [26] Yangying Zhu, Dion S. Antao, Kuang Han Chu, Siyu Chen, Terry J. Hendricks, Tiejun Zhang, Evelyn N. Wang, Surface Structure Enhanced Microchannel Flow Boiling, J. Heat Transfer 138 (9) (2016) 1–13, https://doi.org/10.1115/ 14033497
- [27] A. Sitar, M. Može, M. Crivellari, J. Schille, I. Golobič, Nucleate pool boiling heat transfer on etched and laser structured silicon surfaces, Int. J. Heat Mass Transf. 147 (2020), https://doi.org/10.1016/j.ijheatmasstransfer.2019.118956.
- [28] B.J. Jones, S.V. Garimella, Surface Roughness Effects on Flow Boiling in Microchannels, J. Therm. Sci. Eng. Appl. 1 (4) (2010), https://doi.org/10.1115/ 1.4001804.
- [29] T. Boziuk, M. Smith, A. Glezer, Enhanced boiling heat transfer on micromachined surfaces using acoustic actuation, in: in 2016 15th IEEE Intersociety Conference on Thermal and Thermomechanical Phenomena in Electronic Systems (ITherm), 2016, pp. 994–1001, https://doi.org/10.1109/ITHERM.2016.7517654.
- [30] W. Li, X. Qu, T. Alam, F. Yang, W. Chang, J. Khan, C. Li, Enhanced flow boiling in microchannels through integrating multiple micro-nozzles and reentry microcavities, Appl. Phys. Lett. 110 (1) (2017), https://doi.org/10.1063/ 1.4973495.
- [31] M.J. Rau, S.V. Garimella, Confined Jet Impingement with Boiling on a Variety of Enhanced Surfaces, J. Heat Transfer 136 (10) (2014), https://doi.org/10.1115/ 1.4027942.
- [32] S. Deb, M. Das, D.C. Das, S. Pal, A.K. Das, R. Das, Significance of surface modification on nucleate pool boiling heat transfer characteristics of refrigerant R-141b, Int. J. Heat Mass Transf. 170 (2021), 120994, https://doi.org/10.1016/j. ijheatmasstransfer.2021.120994.
- [33] F. Cui, F. Hong, C. Li, P. Cheng, Two-phase flow instability in distributed jet array impingement boiling on pin-fin structured surface and its affecting factors, Int. J. Heat Mass Transf. 143 (2019), 118495, https://doi.org/10.1016/j. iiheatmasstransfer 2019 118495
- [34] F.L. Cui, F.J. Hong, P. Cheng, Comparison of normal and distributed jet array impingement boiling of HFE-7000 on smooth and pin-fin surfaces, Int. J. Heat Mass Transf. 126 (2018) 1287–1298, https://doi.org/10.1016/j. iiheatmasstransfer.2018.06.058.
- [35] C.H. Hoang, S. Rangarajan, S. Khalili, B. Ramakrisnan, V. Radmard, Y. Hadad, S. Schiffres, B. Sammakia, Hybrid microchannel/multi-jet two-phase heat sink: A benchmark and geometry optimization study of commercial product, Int. J. Heat Mass Transf. 169 (2021) 120920, https://doi.org/10.1016/j.iiheatmasstransfer.2021.120920.
- [36] Ebullient Aims to Take Liquid Cooling Beyond the HPC Market [Online]. Available: https://datacenterfrontier.com/ebullient-liquid-cooling-beyond-hpc/.
- [37] M.S. El-genk, M. Pourghasemi, Experimental Investigation of Saturation Boiling of HFE-7000 Dielectric Liquid on Rough Copper Surfaces, Therm. Sci. Eng. Prog. (2019) 100428, https://doi.org/10.1016/j.tsep.2019.100428.
- [38] J. Shin, T. Rozenfeld, T. Shockner, A.K. Vutha, Local heat transfer under an array of micro jet impingement using HFE-7000, Appl. Therm. Eng. 158 (August 2018) (2010) 112716. https://doi.org/10.1016/j.org
- (2019) 113716, https://doi.org/10.1016/j.applthermaleng.2019.113716.
 [39] C.H. Hoang, G. Mohsenian, N. Fallatafti, V. Radmard, S. Rangarajan, C. Arvin, K. Sikka, S. Schiffres, B. Sammakia, Effects of Different Coolants on the Cooling Performance of an Impingement Microchannel Cold Plate, in: in 2021 37th Semiconductor Thermal Measurement, Modeling & Management Symposium (SEMI-THERM), 2021, pp. 43–49.
- [40] R.J. Moffat, Describing the uncertainties in experimental results, Exp. Therm. Fluid Sci. 1 (1) (1988) 3–17, https://doi.org/10.1016/0894-1777(88)90043-X.
- [41] W.M. Rohsenow, A Method of Correlating Heat Transfer Data for Surface Boiling Liquids, Trans. ASME 74 (1952) 969.
- [42] M.G. Cooper, Heat Flow Rates in Saturated Nucleate Pool Boiling-A Wide-Ranging Examination Using Reduced Properties, Adv. Heat Transf. vol. 16, no. C (1984) 157–239, https://doi.org/10.1016/S0065-2717(08)70205-3.
- [43] R.A. Buchanan, T.A. Shedd, Extensive parametric study of heat transfer to arrays of oblique impinging jets with phase change, J. Heat Transfer 135 (11) (2013), https://doi.org/10.1115/1.4024625.
- [44] M.K. Sung, I. Mudawar, Single-phase and two-phase cooling using hybrid microchannel/slot-jet module, Int. J. Heat Mass Transf. 51 (15–16) (Jul. 2008) 3825–3839, https://doi.org/10.1016/J.IJHEATMASSTRANSFER.2007.12.015.
- [45] Y. Zhang, B. Liu, J. Wei, B. Sundén, Z. Wu, Heat transfer correlations for jet impingement boiling over micro-pin-finned surface, Int. J. Heat Mass Transf. 126 (2018) 401–413, https://doi.org/10.1016/j.ijheatmasstransfer.2018.04.167.